DIRAC NOTE 2006–06

Parametrization of single particle spectra at the DIRAC kinematic range

M. Zhabitsky
JINR Dubna, Russia

October 12, 2006

Abstract

Shapes of single particle spectra from $p + \mathrm{Ni} \to h^{\pm} X$ (h stands for a mixture of pions, kaons and protons) reaction at 24 GeV/c are presented.

Introduction

The DIRAC analyzes $\pi^+\pi^-$-pairs with small relative momenta Q in their center of mass system in order to find out signal from pionium breakup. One of approaches in analysis does rely on correct MC simulation of $\pi^+\pi^-$-pairs inclusively produced in pNi-collisions, which are background to pairs from pionium break-up. Beside the physics of above processes, the adequate transportation of pions through the spectrometer setup and correct detector response are essential for this MC analysis. These can be tested by simulation of so-called accidental pions pairs or even single pions, followed by comparison of MC sample to experimental distributions of events of interest. This study is concentrated on single particle spectra from $p + \mathrm{Ni} \to h^{\pm} X$ reaction, which are required for this analysis.

1 Acceptance

Acceptance of the setup was defined with GEANT-DIRAC simulation program [2]. Input events were generated according to the following distribution

$$\frac{d^3N_{\rm MC}}{dpd\Theta d\varphi} \propto p\exp(-0.8p), \tag{1}$$

here p, Θ, φ are in spherical system of coordinates with its origin in the center of the target and z-axis along the primary proton beam. Momenta and angles of input events were generated in the range about 10% wider then the actual acceptance of the setup. Then tracks were reconstructed by ARIANE reconstruction program [3]. Acceptance function $G(\vec{p})$ was defined as a ratio of reconstructed distribution over generated one:

$$G^{\pi^-}(p,\Theta,\varphi) = \frac{d^3N^{\rm rec}_{\rm MC}}{dpd\Theta d\varphi}\Big/\frac{d^3N_{\rm MC}}{dpd\Theta d\varphi}. \tag{2}$$

Here we assume that the value of the reconstructed momenta $\vec{p}_{\rm rec}$ is close to the generated one $\vec{p}_{\rm gen}$. Also production at the center of the target is used. Actual dimensions of the beam spot at the target location are $x = 1.6$ mm $y = 3.2$ mm at 2σ level; the divergence of the beam is about 1 mrad [4]. Angular acceptance is defined by the collimator placed 3.5 m from the target, therefore divergence due to the size of the beam spot is also less than 1 mrad.

An event is called reconstructed if following criteria are fulfilled:

- track is reconstructed in DC;
- no hit in Muon hodoscope;
- hit with proper timing (± 4 ns) in PreShower;
- reconstructed value of momenta is close to the generated one $|p_{\rm rec} - p_{\rm gen}| < 0.1$GeV/c;
- angular deviation is also small: angle between $\vec{p}_{\rm rec}$ and $\vec{p}_{\rm gen}$ is less than 0.01.

Acceptance is mainly defined by the collimator (fig. 1.b), magnetic field and geometry of downstream detectors (fig. 1.a). Actual value of acceptance for MC π^- events in "inner" part of acceptance is about 80% (fig. 1.d) Last number takes into account efficiencies of downstream detectors, probability of track reconstruction in DCs and probability of pion decay in flight. Mean decay length of pion in laboratory frame $\lambda = c\tau p/m$ exceeds 80 m, where as its path length between target and muon hodoscope is less than 20 m. Losses due to decay increase up to 10% for pions with lower momenta (see fig. 3).

Applied criteria correspond to experimental cuts which suppress background events on the trigger level and/or on the reconstruction stage. Suppression factors of different criteria are presented in table 1. Momentum dependence of the above criteria are in fig. 2. From fig. 2 one can see that some tracks with momenta lower than 1.5 GeV/c or greater than 5 GeV/c can be reconstructed in Drift Chambers but do not cross PreShower plane. As signal from PreShower was required in T1 trigger, this limits the range where inclusive spectra can be defined in the experiment. Other origin of losses is an interaction of pions with the Al frame of Cherenkov detector, which is 3 cm high and 20-40 cm thick along the

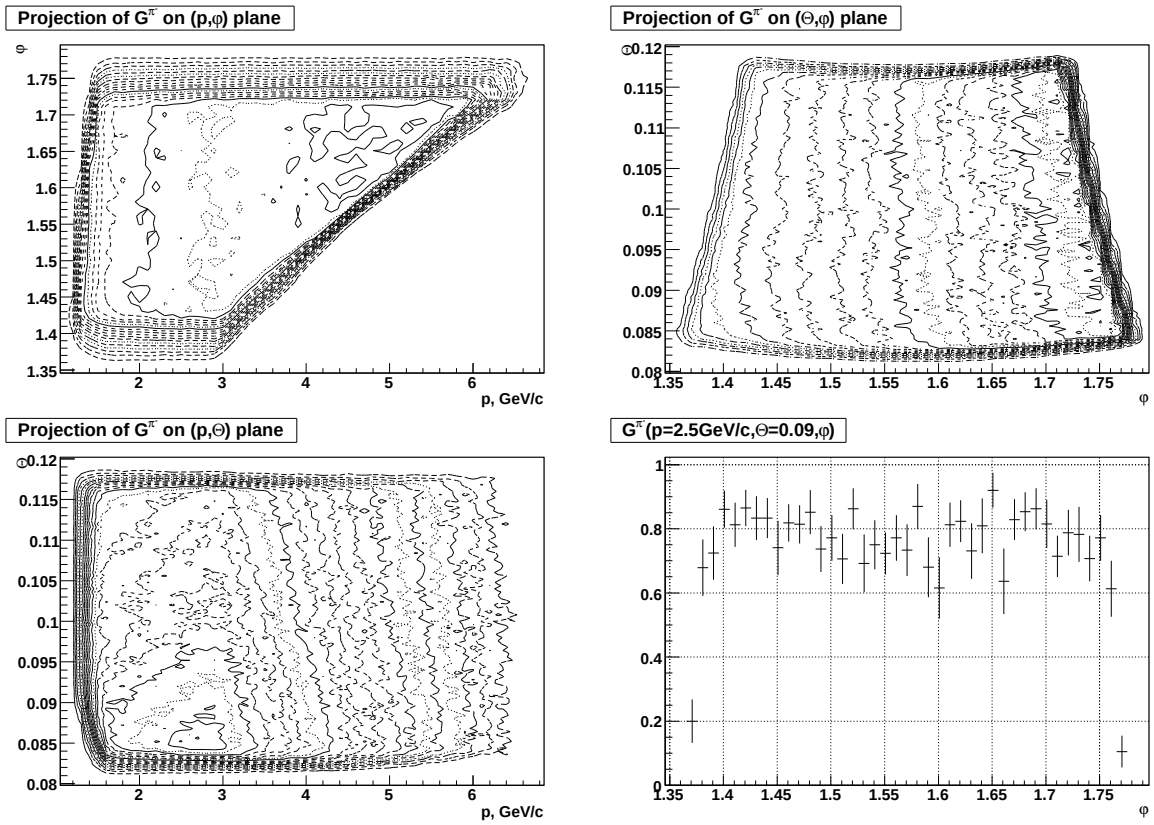

Figure 1: Projections of $G^{\pi^-}(p, \Theta, \varphi)$ acceptance on planes: a – (p, φ), b – (Θ, φ), c – (p, Θ). d – $G^{\pi^-}(p = 2.5\,\mathrm{GeV}/c, \Theta = 0.09, \varphi)$.

Table 1: Suppression factors of different criteria in MC

		π^-		π^+		K^+		p	
	criteria	N. ev.		N. ev.		N. ev.		N. ev.	
1.	DC(TmTrxDC)	2520168	1	508083	1	295804	1	510357	1
2.	1. & $\lvert\Delta t(\mathrm{PrSh})\rvert < 4$ ns	2335788	0.93	471385	0.93	255196	0.86	457461	0.90
3.	1. & no Muons	2279180	0.90	459822	0.91	272700	0.92	506504	0.99
4.	2. & no Muons	2096641	0.83	423461	0.83	232557	0.79	453782	0.89
5.	4. & $\lvert\Delta\lvert p\rvert\rvert < 0.1\,\mathrm{GeV}/c$	2057148	0.82	415533	0.82	222523	0.75	446405	0.87
6.	4. & $\lvert\Delta\Theta\rvert < 0.01$	2061575	0.82	416314	0.82	225296	0.76	445425	0.87
7.	5. & $\lvert\Delta\Theta\rvert < 0.01$	2047758	0.81	413620	0.81	221369	0.75	443613	0.87

secondary particles path and stands in the central horizontal plane of the spectrometer. This leads to a pronounced dip in experimental data due to loss of signal in PreShower which is in T1 trigger. This effect was not reproduced numerically in MC, so events with Θ around 0.1 has to be removed from analysis.

From figure 2.b one can conclude that applied cuts on difference between generated and reconstructed values of momenta suppress 2-4% of MC events. Slope on p due to these cuts is less than $0.004\,[\mathrm{GeV}/c]^{-1}$ between 2 and 5 GeV/c.

Acceptance functions for positive pions $G^{\pi^+}(p, \Theta, \varphi)$ and protons $G^{\mathrm{p}}(p, \Theta, \varphi)$ are defined in the similar way. We introduce space Ω^{π^-} where acceptance is high:

$$\Omega^{\pi^-} = \left\{ p, \Theta, \varphi : \quad G^{\pi^-}(p, \Theta, \varphi) > 0.4 \right\} \tag{3}$$

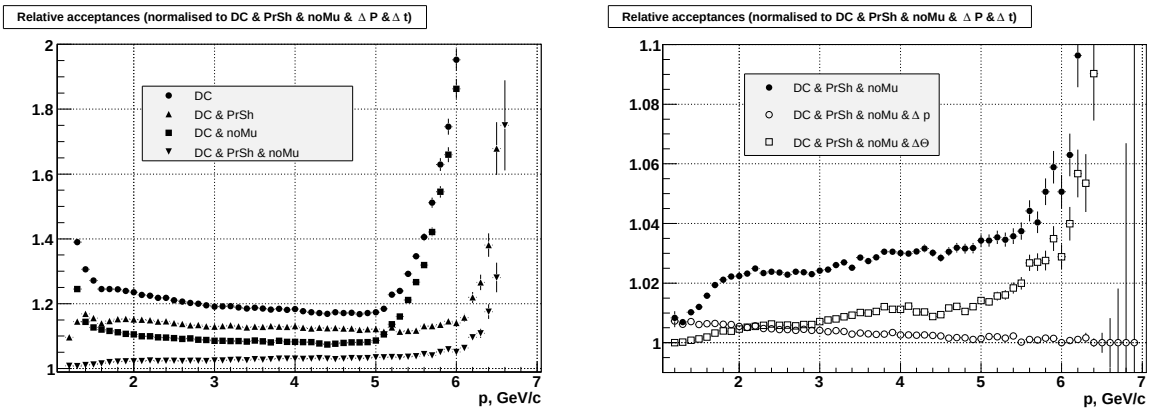

Figure 2: Projections of π^- relative acceptances on p for different selection criteria

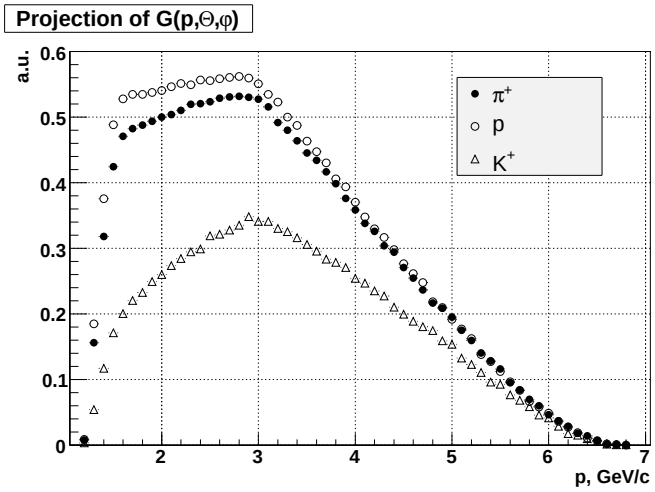

Figure 3: Acceptance $G(p, \Theta, \varphi)$ as a function of momenta for π^+, K^+ and protons.

1.1 Acceptance with advanced tracking ("noup")

We will also define acceptance function $G^{\pi^-}_{\rm noup}(p,\Theta,\varphi)$ for MC events reconstructed by the more detailed track reconstruction procedure (results are stored in the common block FitTrkDC of ARIANE, only beam spot position and DC information are used)[1]. It is defined with similar cuts as $G^{\pi^-}(p,\Theta,\varphi)$. Suppression factors of different criteria are presented in table 2. Momentum dependence of the above criteria are in fig. 4. Ratio of $G^{\pi^-}_{\rm noup}(p,\Theta,\varphi)$ over $G^{\pi^-}(p,\Theta,\varphi)$ as a function of momenta is presented in fig. 5. Events are rejected for two main reasons: track does not point to the beam spot (± 2 cm in vertical direction) or it is not possible to propagate track in DC backward through the magnetic field for given track parameters. These can happen either due to pion decay in flight or incorrect map of the magnetic field. Last reason is responsible for the pronounced inefficiency between 3 and 4 GeV/c (see fig. 5).

Table 2: Suppression factors of different criteria in MC

		π^-		π^+	
	criteria	N. ev.		N. ev.	
0.	DC(TmTrxDC)	2520168	1.13	509170	1.14
1.	DC(FitTrkDC)	2232956	1	448318	1
2.	1. & $\lvert\Delta t(\mathrm{PrSh})\rvert < 4$ ns	2067028	0.93	415414	0.93
3.	1. & no Muons	2096344	0.94	421212	0.94
4.	2. & no Muons	1931844	0.87	388561	0.87
5.	4. & $\lvert\Delta\lvert p\rvert\rvert < 0.1$ GeV/c	1925497	0.86	387272	0.86
6.	4. & $\lvert\Delta\Theta\rvert < 0.01$	1928467	0.86	387850	0.87
7.	5. & $\lvert\Delta\Theta\rvert < 0.01$	1924410	0.86	387051	0.86

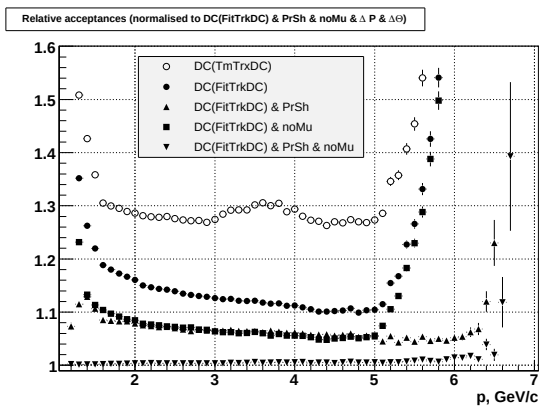

Figure 4: Projections of π^- relative acceptances on p for different selection criteria.

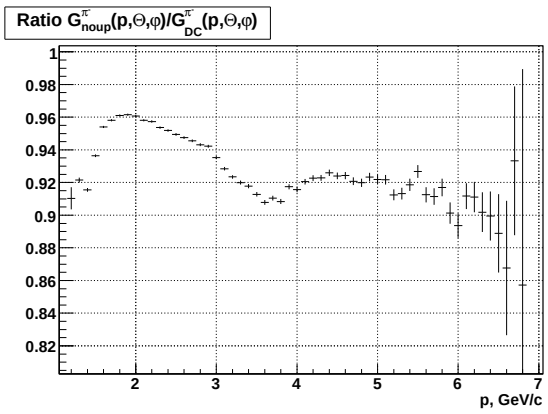

Figure 5: Ratio $G^{\pi^-}_{\rm noup}(p,\Theta,\varphi)\Big/ G^{\pi^-}(p,\Theta,\varphi)$ as a function of momenta.

[1]Hereafter we will denote results with simplified tracking in DC (TmTrxDC) as "DC", more detailed fitting (FitTrkDC) as "noup" and results with SFD detector as "DC&SFD"

1.2 Acceptance with forward detectors (DC&SFD)

We will also define acceptance function $G^{\pi^-}_{\mathrm{SFD}}(p,\Theta,\varphi)$ for MC events reconstructed in forward detectors (only SFD used, without background simulation). It is defined with similar cuts as $G^{\pi^-}(p,\Theta,\varphi)$. Momentum dependence of the above criteria and their suppression factors are in fig. 6. Between 1.5 and 5 GeV/c shape of $G^{\pi^-}_{\mathrm{SFD}}(p,\Theta,\varphi)$ is similar to the shape of acceptance function with downstream detectors only (see fig. 8).

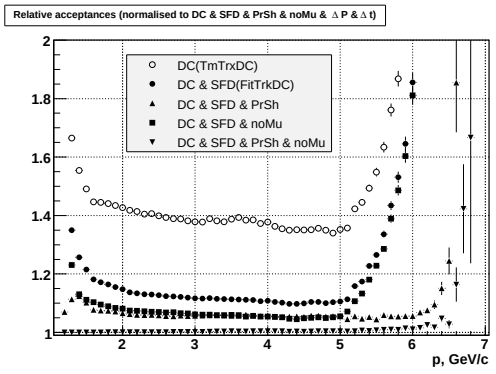

		π^-	
	criteria	N. ev.	
0.	DC(TmTrxDC)	2520168	1.24
1.	DC+SFD(FitTrkDC)	2028689	1
2.	1. & $\lvert\Delta t(\mathrm{PrSh})\rvert < 4$ ns	1876736	0.93
3.	1. & no Muons	1914851	0.94
4.	2. & no Muons	1764142	0.87
5.	4. & $\lvert\Delta \lvert p\rvert\rvert < 0.1$ GeV/c	1761155	0.87
6.	4. & $\lvert\Delta\Theta\rvert < 0.01$	1763844	0.87
7.	5. & $\lvert\Delta\Theta\rvert < 0.01$	1761052	0.87

Figure 6: Projections of π^- relative acceptances on p for different selection criteria.

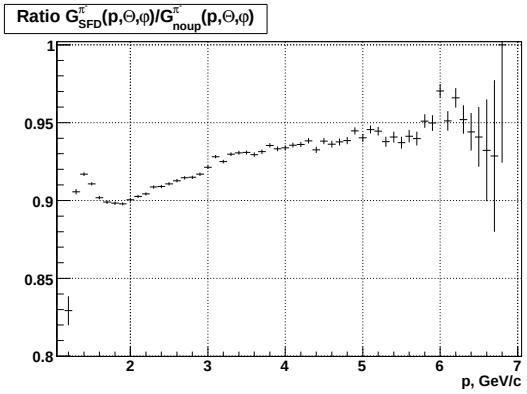

Figure 7: $G^{\pi^-}_{\mathrm{SFD}}(p,\Theta,\varphi)\Big/ G^{\pi^-}_{\mathrm{noup}}(p,\Theta,\varphi)$ as a function of momenta.

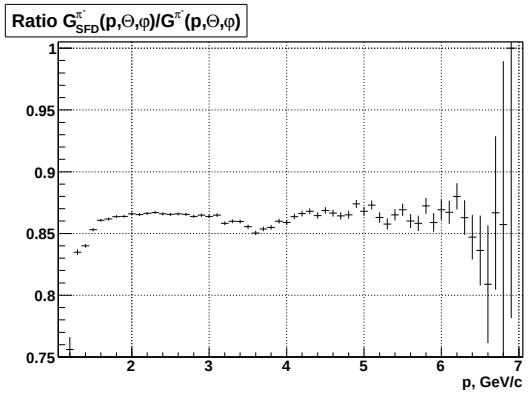

Figure 8: $G^{\pi^-}_{\mathrm{SFD}}(p,\Theta,\varphi)\Big/ G^{\pi^-}(p,\Theta,\varphi)$ as a function of momenta.

2 Experimental distributions

The goal of the DIRAC experiment is to study $\pi^+\pi^-$-pairs with small relative momenta Q in their center of mass system. For this reason all working triggers select pairs and even make decision depending on topology of hits specific to small Q. In 2003 the dedicated run (No. 6371) was taken to test trigger system. In overall 2 millions of "T1 $\pi^+\pi^-$ without coplanarity" events were taken. Here trigger T1 = $(\mathrm{VH\&HH\&PrSh\&}\overline{\mathrm{Ch}})\big|_+$ & $(\mathrm{VH\&HH\&PrSh\&}\overline{\mathrm{Ch}})\big|_-$ stands for coincidence of pion track candidates in positive and negative arms. If one selects events with 2 separated in time tracks from different proton-nucleus interactions (so-called accidental coincidences) then detected distributions in each arm correspond to inclusive production of positive or negative hadrons in proton collisions with nuclear target (pNi $\to h^{\pm}X$), but without inclusive pair production (pNi $\to h^+h^-X$), when both particles enter the Spectrometer acceptance. Rate of such accidental events is proportional to the product of corresponding total cross-sections. These accidental events can be identified by selecting proper time difference between detected positive and negative particles (fig. 9). Time difference distribution is asymmetric due to time-correlated protons, for this reason only events in $[-15, -5]$ ns range were analyzed.

Counting rates per element in vertically oriented hodoscopes depend on covered momentum range (high and low occupancies differ by a factor 2.0−2.2). It was experimentally shown [5] that within 1% accuracy there are no losses due to this difference either on the trigger level or on the reconstruction stage.

Below we will separately analyze distributions for positive and negative hadrons.

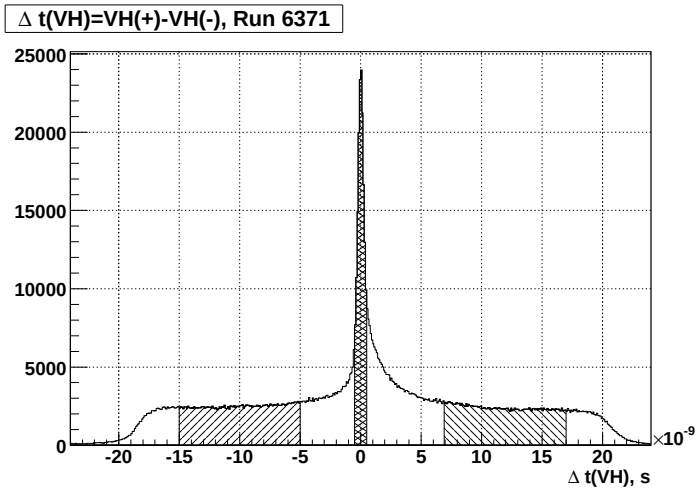

Figure 9: Time difference between positive and negative particles (assuming both of them pions).

2.1 $p + \mathrm{Ni} \to h^- X$

In experimental data we selected only accidental events in the range $[-15, -5]$ ns with tracks in both positive and negative arms reconstructed. Corresponding hit with proper timing in PrSh and absence of signals in Muon hodoscope in the region around the track path were required. 215547 events fulfilled the above criteria (MC sample used for the acceptance definition is ten times more). Effect of above cuts are presented in fig. 10.

Then shape of production differential cross section can be estimated:

$$\frac{d^3N}{dpd\Theta d\varphi} = \frac{1}{G^{\pi^-}(p,\Theta,\varphi)} \frac{d^3N^{\mathrm{det}}}{dpd\Theta d\varphi}, \tag{4}$$

$$\frac{d^2N}{dpd\Theta} = \omega(p,\Theta) \int\limits_{\Omega^{\pi^-}} \frac{d^3N}{dpd\Theta d\varphi} d\varphi, \tag{5}$$

where $\omega(p,\Theta) = \dfrac{2\pi}{\Delta\varphi(p,\Theta)}$, $\Delta\varphi$ — part of azimuthal angle inside of Ω^{π^-} for a given values of p and Θ. Here we assume that after the correction to acceptance we will get flat distribution on azimuthal angle φ within Ω^{π^-} (see fig. 11). We will call this strategy "G". While using acceptance function G^{π^-} we neglect admixture of K^- which are about 5% abundant [8], but has similar shape. In detected events their admixture is even lower due to shorter kaon lifetime (fig. 3).

Alternative way is to assume some reasonable shape of the production differential cross section $\dfrac{d^2N^{i-1}_{\mathrm{MC}}}{dpd\Theta}$, then obtain in MC corresponding "detected" shape $\dfrac{d^2N^{i-1\,\mathrm{det}}_{\mathrm{MC}}}{dpd\Theta}$. Last distribution can be compared to experimental results $\dfrac{d^2N^{\mathrm{det}}}{dpd\Theta}$. If one adjusts initial shape of the production differential cross section

$$\frac{d^2N^{i}_{\mathrm{MC}}}{dpd\Theta} = \frac{d^2N^{i-1}_{\mathrm{MC}}}{dpd\Theta} \frac{\dfrac{d^2N^{\mathrm{det}}}{dpd\Theta}}{\dfrac{d^2N^{i-1\,\mathrm{det}}_{\mathrm{MC}}}{dpd\Theta}} \tag{6}$$

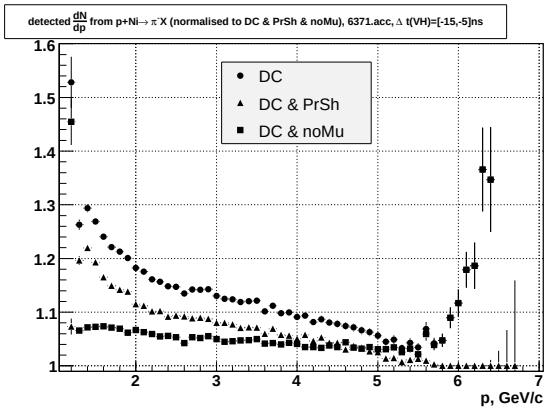

	criteria	N. events	
1.	DC(1 track)	250214	1
2.	1. & $\lvert\Delta t(\mathrm{PrSh})\rvert < 4$ ns	237815	0.95
3.	1. & no Muons	227788	0.91
4.	2. & no Muons	215547	0.86

Figure 10: Relative shape of $\dfrac{dN^{\mathrm{det}}}{dp}$ for different selection criteria.

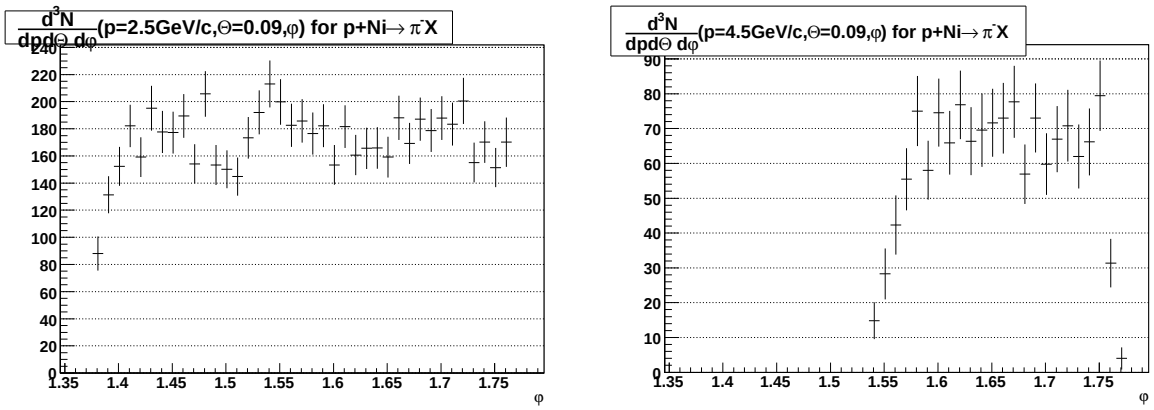

Figure 11: $\frac{d^3N}{dpd\Theta d\varphi}$ as a function of azimuthal angle φ.

and repeat MC step, then by iteration the shape of the production differential cross section, which reproduces in MC the experimental distribution, can be obtained. We will call this strategy "I". In our analysis shape from formula (1) was used as $\frac{d^2N^0_{\rm MC}}{dpd\Theta}$ and only one iteration was done. Therefore this method allow us to test validity of assumptions of strategy "G": uniformity of the obtained production differential cross section over azimuthal angle and restriction of analysis only to events inside space Ω^{π^-}.

Usually the double differential cross section $\frac{d^2N}{dpd\Theta}$ is parametrized by either Sanford-Wang parametrization [7] or Badhwar parametrization [6]. We used only Badhwar parametrization of LIDCS for $p+p\to\pi^-X$ as it has less free parameters (for details see Appendix A). Fits were performed over 2 regions $\{p\in[1.5,5]\text{GeV/c},\Theta\in[0.085,0.095]\}$ and $\{p\in[1.5,5]\text{GeV/c},\Theta\in[0.105,0.115]\}$ with $A_{\rm cs}$, B, C_1, C_2 and C_3 as free parameters (see fit results in table 3). Slices of the production cross-section with superimposed fits are presented for fixed values of Θ (fig. 12) and fixed values of momenta (fig. 13). Parameters C_1, C_2 and C_3 are polynomial coefficients from term $C_1+C_2p_\perp+C_3p_\perp^2$. In DIRAC $p_\perp$

Table 3: Fit parameters for π^- production

Particle		B	C_1	C_2 $[(\text{GeV}/c)^{-1}]$	C_3 $[(\text{GeV}/c)^{-2}]$	χ^2/NDF
$\{p\in[1.5,5]\text{GeV/c},\Theta\in[0.085,0.095]\}$ and $\{p\in[1.5,5]\text{GeV/c},\Theta\in[0.105,0.115]\}$						
π^-	G	3.75 ± 0.19	14.8 ± 0.6	-17.3 ± 2.4	14.5 ± 2.6	2135/1903
π^-	G^0	2.53 ± 0.13	10.81 ± 0.24	0.0	0.0	2171/1905
π^-	I	3.40 ± 0.25	13.1 ± 0.5	-9.5 ± 3.0	6.3 ± 3.1	2105/1903
π^-	I^0	2.55 ± 0.13	10.77 ± 0.24	0.0	0.0	2135/1905
$\{p\in[2.0,5]\text{GeV/c},\Theta\in[0.085,0.095]\}$ and $\{p\in[2.0,5]\text{GeV/c},\Theta\in[0.105,0.115]\}$						
π^-	G	4.19 ± 0.24	15.4 ± 0.7	-20.9 ± 2.7	17.2 ± 2.7	1851/1638
π^-	G^0	2.62 ± 0.14	10.4 ± 0.3	0.0	0.0	1867/1640
π^-	I	4.17 ± 0.24	15.1 ± 0.7	-18.7 ± 2.7	14.1 ± 2.7	1827/1638

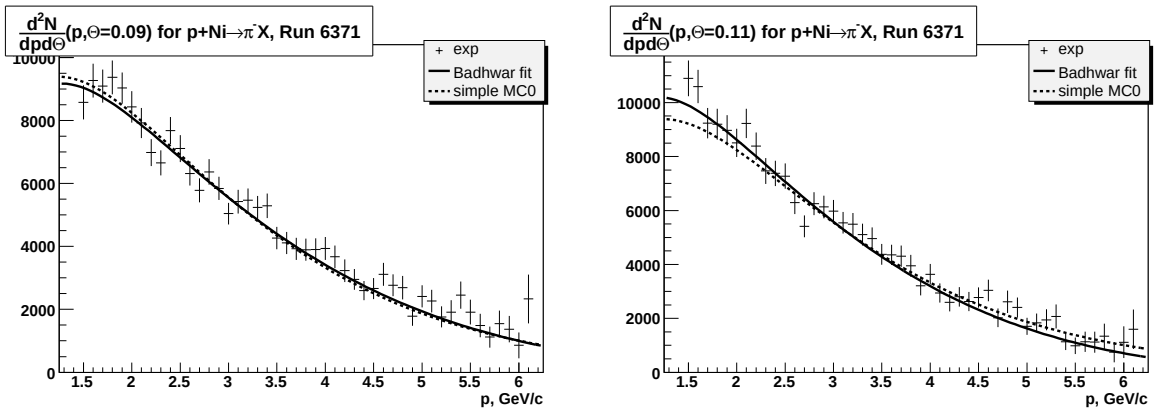

Figure 12: $\frac{d^2N}{dpd\Theta}\left(p + \mathrm{Ni} \to \pi^- X\right)$ for fixed values of Θ.

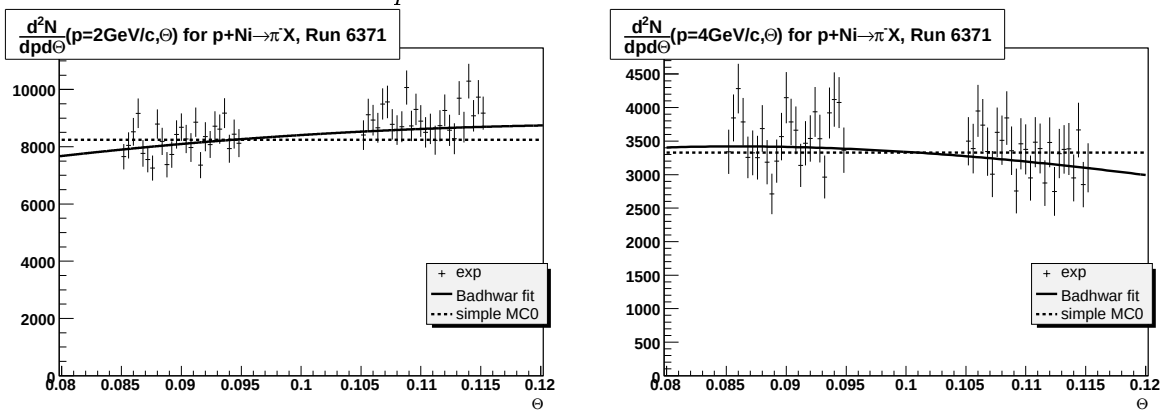

Figure 13: $\frac{d^2N}{dpd\Theta}\left(p + \mathrm{Ni} \to \pi^- X\right)$ for fixed values of p.

belongs to $0.1 - 0.5\,\mathrm{GeV}/c$ range, so C_2 and C_3 correspond to rather small terms. For future reference we will produce fits G^0 and I^0 with $C_2 = C_3 = 0$.

It is expected, that the production cross section (dN/dp) has its maximum near $1\,\mathrm{GeV}/c$. To test stability of fit results another fit was performed for $p \in [2.0, 5]\mathrm{GeV/c}$ (see fit results in table 3), which provided a similar shape (within 3%) in the accessible kinematic range (fig. 14). Also a fit over the distribution obtained by strategy "I" provides close result (fig. 15).

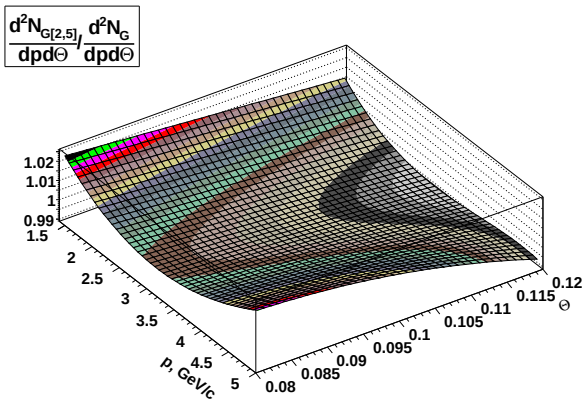

Figure 14: $\dfrac{d^2N_{\mathrm{G}[2,5]}}{dpd\Theta} \Big/ \dfrac{d^2N_{\mathrm{G}}}{dpd\Theta}$.

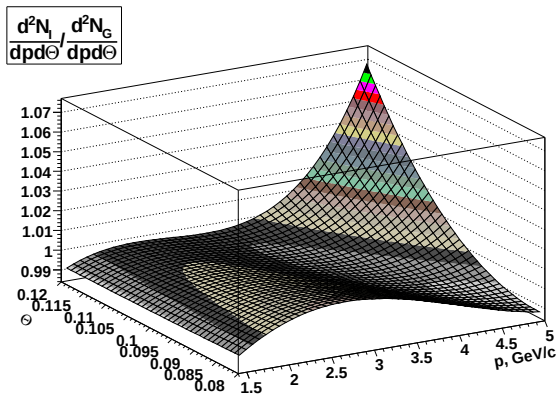

Figure 15: $\dfrac{d^2N_{\mathrm{I}}}{dpd\Theta} \Big/ \dfrac{d^2N_{\mathrm{G}}}{dpd\Theta}$.

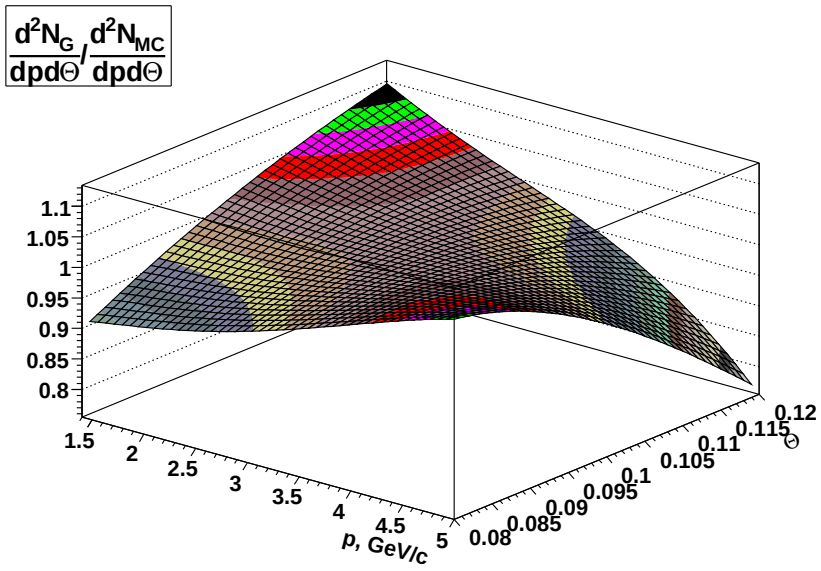

Figure 16: $\dfrac{d^2N_{\mathrm{G}}}{dpd\Theta} \Big/ \dfrac{d^2N_{\mathrm{MC}}}{dpd\Theta}$ $\left(p + \mathrm{Ni} \to \pi^- X\right)$ for the DIRAC kinematic range.

MC based on formula (1) is already a good approximation for the shape of the double differential production cross-section in the kinematic range of the DIRAC setup (fig. 16): the maximal relative difference between its shape and the "realistic" shape of the double differential production cross-section is less then 24% in the range $p \in [1.5, 5]$ GeV/c and $\Theta \in [0.08, 0.12]$. Actually this simple shape was chosen as it fits the median line ($\Theta = 0.1$) of the "realistic" shape with relative difference less than 3%.

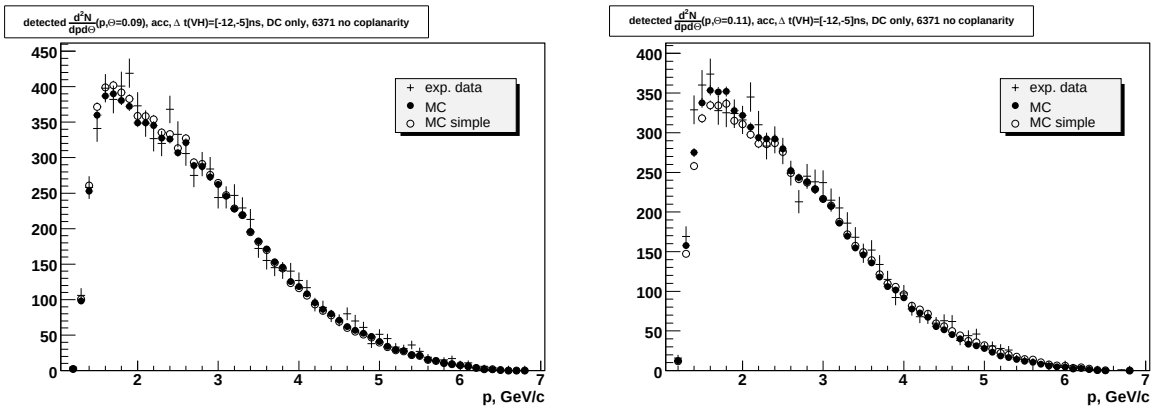

Figure 17: Detected $\dfrac{d^2N^{\mathrm{det}}}{dpd\Theta}$ for fixed values of Θ.

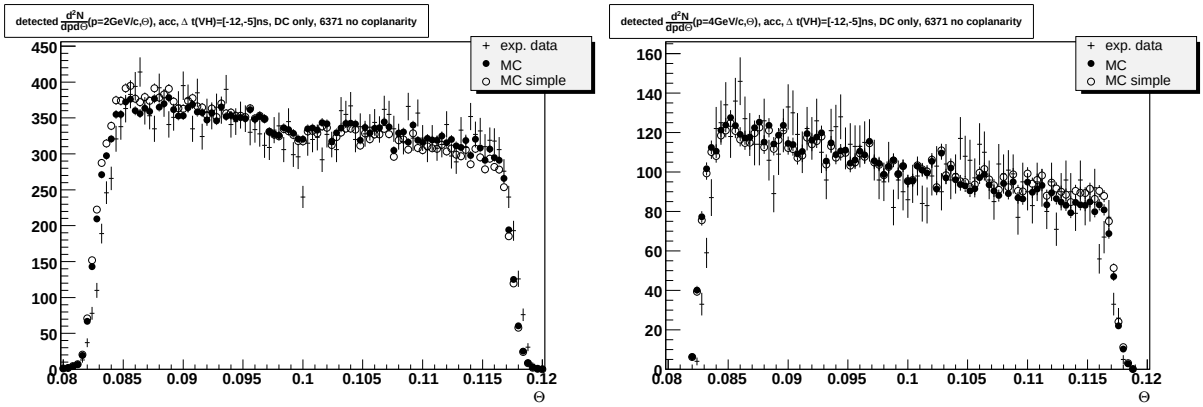

Figure 18: Detected $\dfrac{d^2N^{\mathrm{det}}}{dpd\Theta}$ for fixed values of p.

For cross-check the following MC test was performed: input events for GEANT-DIRAC were generated according to the Badhwar representation of LIDCS with obtained parameters, then events were reconstructed by the ARIANE. Calculated double-differential distributions have been compared to experimental ones. Their slices for fixed values of Θ are in fig. 17 and for fixed values of momenta are in fig. 18.

2.1.1 $p + \mathrm{Ni} \to h^- X$: advanced tracking

Results of the more advanced tracking with Drift Chambers and more detailed map of the magnetic field ("noup") are presented in fig. 19 and table 4. Additional information about spectra can be obtained with forward detectors. If ARIANE manages to find out a hit candidate with proper timing in SFD for a downstream track, then such events can be used to build another set of distributions on the target (see fig. 20 and table 5).

While comparing obtained production distributions with simplified and more advanced tracking (fig. 21, 22) one can conclude that the difference between shapes in the low momenta region can not be explained only by the difference in corresponding acceptance functions (fig. 5, 8). Most presumably this region contains pions which appeared not in the target center: either as a decay product of long-lived particles (mainly kaons) or in interactions of the beam halo with the target, or pions burn/re-scattered in setup parts near the target. These events are suppressed when the requirement of a track to intersect the central part of the target is applied. It is worth to note that advanced reconstruction with and without forward detectors reproduce the same production distribution on target (fig. 24). For completeness the reconstructed shape $\frac{d^2 N_{\mathrm{DC\&SFD}}}{dpd\Theta}$ is shown in fig. 25.

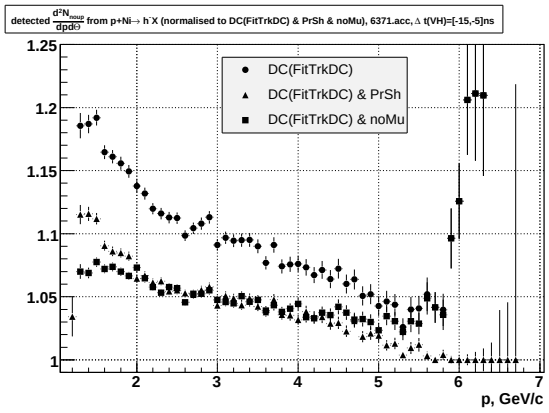

	criteria	N. events	
1.	DC(TmTrxDC)	250214	1.47
2.	DC(FitTrkDC)	170312	1
3.	2. & $\lvert\Delta t(\mathrm{PrSh})\rvert < 4$ ns	161540	0.95
4.	2. & no Muons	161014	0.95
5.	3. & no Muons	152344	0.90

Figure 19: Relative shape of $\frac{dN^{\mathrm{det}}_{\mathrm{noup}}}{dp}$ for different selection criteria.

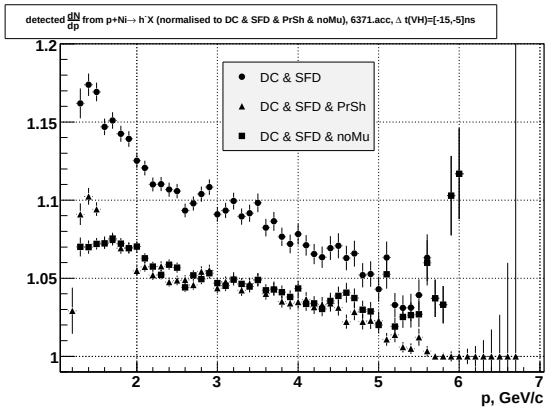

	criteria	N. events	
1.	DC(TmTrxDC)	250214	1.58
2.	DC&SFD(FitTrkDC)	158009	1
3.	2. & $\lvert\Delta t(\mathrm{PrSh})\rvert < 4$ ns	149881	0.95
4.	2. & no Muons	150260	0.95
5.	3. & no Muons	142216	0.90

Figure 20: Relative shape of $\frac{dN^{\mathrm{det}}_{\mathrm{DC\&SFD}}}{dp}$ for different selection criteria.

Table 4: Fit parameters for π^- production (DC(FitTrkDC))

Particle		B	C_1	C_2 $[(\mathrm{GeV}/c)^{-1}]$	C_3 $[(\mathrm{GeV}/c)^{-2}]$	χ^2/NDF
$\{p \in [1.5,5]\mathrm{GeV/c}, \Theta \in [0.085,0.095]\}$ and $\{p \in [1.5,5]\mathrm{GeV/c}, \Theta \in [0.105,0.115]\}$						
π^-	G	2.70 ± 0.22	9.5 ± 0.6	3.7 ± 2.7	-5.7 ± 2.9	1900/1903
π^-	G^0	2.70 ± 0.15	10.2 ± 0.3	0.0	0.0	1905/1905

Table 5: Fit parameters for π^- production (DC&SFD)

Particle		B	C_1	C_2 $[(\mathrm{GeV}/c)^{-1}]$	C_3 $[(\mathrm{GeV}/c)^{-2}]$	χ^2/NDF
$\{p \in [1.5,5]\mathrm{GeV/c}, \Theta \in [0.085,0.095]\}$ and $\{p \in [1.5,5]\mathrm{GeV/c}, \Theta \in [0.105,0.115]\}$						
π^-	G	3.13 ± 0.23	10.3 ± 0.7	-2.1 ± 2.8	0.9 ± 2.9	1942/1903
π^-	G^0	2.89 ± 0.16	9.7 ± 0.3	0.0	0.0	1945/1905
π^-	I	3.01 ± 0.23	10.5 ± 0.6	-1.3 ± 2.7	-0.4 ± 2.9	1898/1903
π^-	I^0	2.76 ± 0.16	10.1 ± 0.3	0.0	0.0	1903/1905

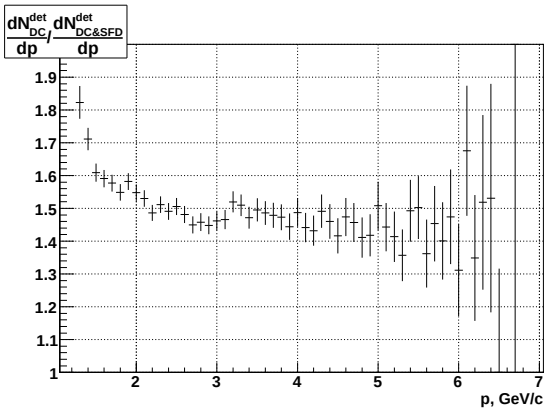

Figure 21: $\dfrac{dN^{\mathrm{det}}_{\mathrm{DC}}}{dp} \Big/ \dfrac{dN^{\mathrm{det}}_{\mathrm{DC\&SFD}}}{dp}$.

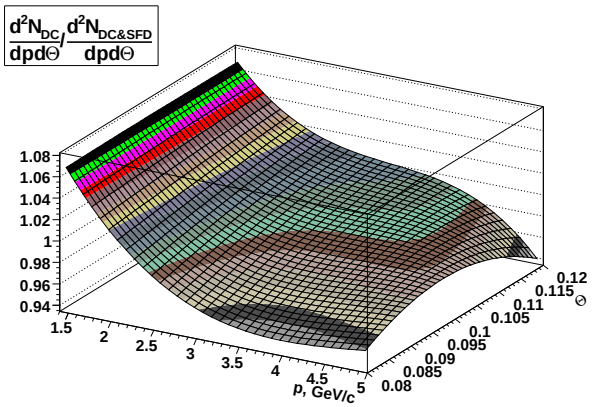

Figure 22: $\dfrac{d^2N_{\mathrm{DC}}}{dpd\Theta} \Big/ \dfrac{d^2N_{\mathrm{DC\&SFD}}}{dpd\Theta}$.

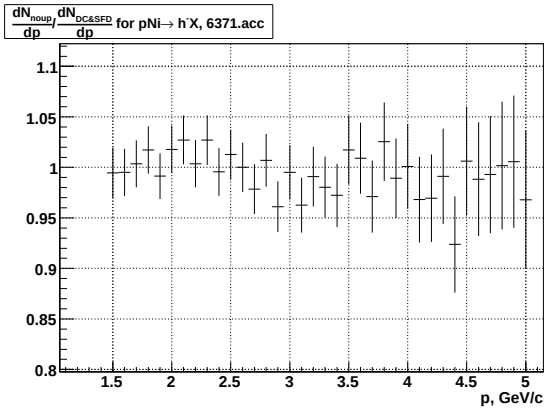

Figure 23: $\dfrac{dN_{\mathrm{noup}}}{dp} \Big/ \dfrac{dN_{\mathrm{DC\&SFD}}}{dp}$.

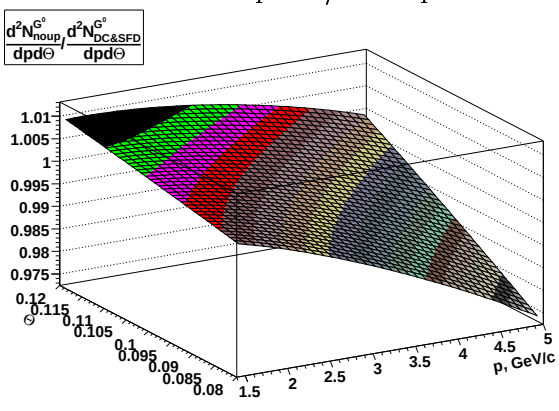

Figure 24: $\dfrac{d^2N^{G^0}_{\mathrm{noup}}}{dpd\Theta} \Big/ \dfrac{d^2N^{G^0}_{\mathrm{DC\&SFD}}}{dpd\Theta}$.

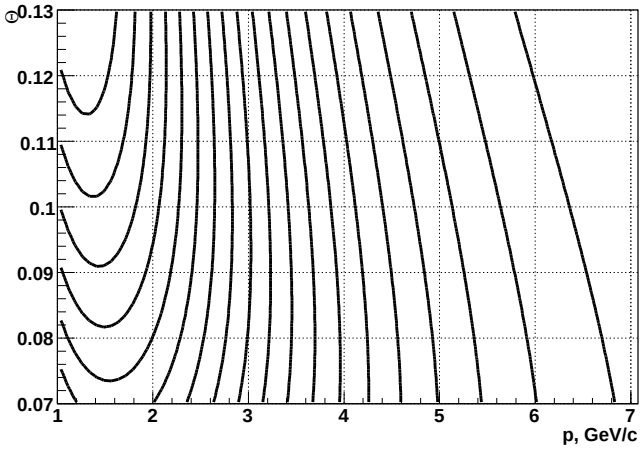

Figure 25: $\frac{d^2N_{\mathrm{DC\&SFD}}}{dpd\Theta}$ for pNi $\to h^-X$.

We will compare the distribution $\frac{d^2N_{\mathrm{DC\&SFD}}}{dpd\Theta}$ to the shape of negative pion production by 24GeV/c protons from Cu [8]. The later experiment covered the secondary momentum range $4-18$ GeV/c and the angular range $17-127$ mrad. Angular acceptance of the experiment $\Delta\Omega = 7.62\cdot 10^{-6}$ sr. Phase space was scanned by means of magnet which deflected produced secondary particles into the setup. Their results were tabulated for the measured Lorentz invariant one particle distribution functions $\omega(p,\Theta)$ defined by

$$d^2N = \frac{1}{\sigma_a}\frac{\delta^2\sigma}{\delta p\delta\Omega}dpd\Omega = \omega(p,\Theta)\frac{p^2dpd\Omega}{2E}, \tag{7}$$

where $\frac{\delta^2\sigma}{\delta p\delta\Omega}$ is the differential production cross section, σ_a is the absorption cross section for pCu collisions, Ω is the solid angle. Three corrections have been applied to the measurements:

- for absorption of the produced pions along the spectrometer;
- for decay of pions along the spectrometer;
- subtraction of the empty target background.

Uncertainties in results were dominated by systematic errors, which included the irreproducibility of a given setup settings (about 5%) and by the uncertainties in the corrections applied (2-5% depending on momentum).

We will introduce

$$\frac{d^2N_{\mathrm{Eichten}}}{dpd\Theta} = \frac{1}{\sigma_a}\frac{d^2\sigma}{dpd\Theta} = \omega(p,\Theta)\frac{\pi p^2\sin\Theta}{E}. \tag{8}$$

The fit parameters of the above function by the Badhwar parametrization of LIDCS for $p+p\to\pi^-X$ are presented in table 6 (see also fig. 26). The double integral of this Badhwar parametrization over the total kinematic region on momenta and angle gives

Table 6: Fit parameters for π^- production in $\mathrm{p} + \mathrm{Cu} \to \pi^- X$ [8]

Particle	A_{cs}/σ_a $[(\mathrm{GeV}^2/c^3)^{-1}]$	B	C_1	C_2 $[(\mathrm{GeV}/c)^{-1}]$	C_3 $[(\mathrm{GeV}/c)^{-2}]$	χ^2/NDF
			$p \in [4, 22]\mathrm{GeV/c}, \Theta \in [0.017, 0.127]$			
π^-	1.59 ± 0.07	3.46 ± 0.14	4.78 ± 0.15	-1.3 ± 0.6	1.6 ± 0.5	$106/17^*$
π^-	1.63 ± 0.04	3.55 ± 0.05	4.53 ± 0.04	0.0	0.0	$127/19^*$
			$p \in [4, 6]\mathrm{GeV/c}, \Theta \in [0.050, 0.127]$			
π^-	2.4 ± 1.1	3.3 ± 1.2	7.1 ± 2.6	-4.9 ± 8.2	4.7 ± 4.7	$0.36/2^*$
π^-	2.36 ± 0.19	3.30 ± 0.18	5.9 ± 0.5	0.0	0.0	$3.5/4^*$

* to all data points 5% relative errors were attributed

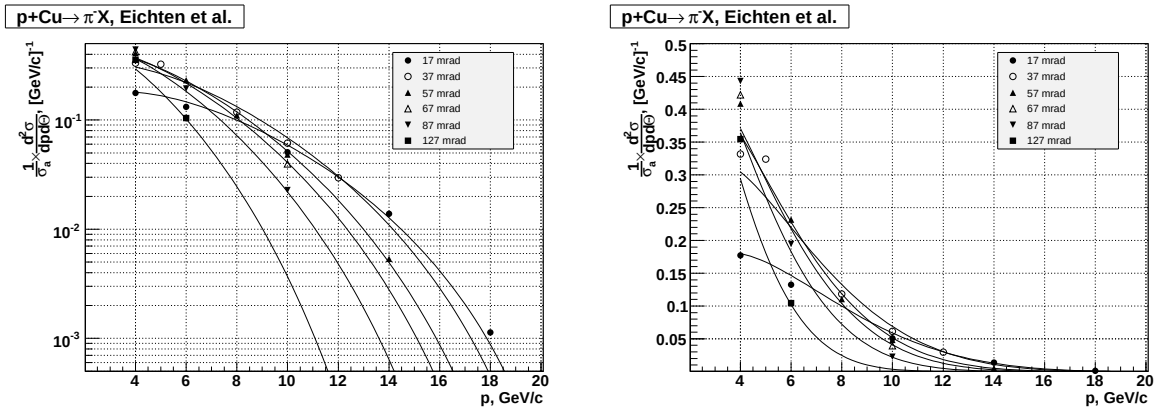

Figure 26: $\dfrac{d^2N_{\mathrm{Eichten}}}{dpd\Theta}$ fitted.

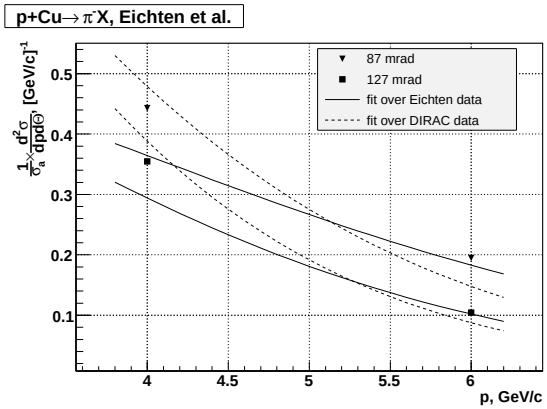

Figure 27: $\dfrac{d^2N_{\mathrm{Eichten}}}{dpd\Theta}$ in the range $p \in [4, 6]\mathrm{GeV}/c$ and $\Theta \in [80, 130]\mathrm{mrad}$.

0.93 ± 0.05. It is clear that the Badhwar parametrization (fit over the whole sample) does not reproduce measured points for momenta between 4 and 6 GeV/c.

In fig. 27 data by Eichten at al. [8] is compared to the Badhwar parametrization of $\dfrac{d^2N_{\mathrm{DC\&SFD}}}{dpd\Theta}$ detected by DIRAC in the kinematic region covered by both experiments.

2.2 $p + \mathrm{Ni} \to h^+X$

In experimental data we selected only accidental events in the range $[-15, -5]$ ns with tracks in both positive and negative arms reconstructed. Corresponding hit with proper timing in PrSh and absence of signals in Muon hodoscope in the region around the track path were required. 220259 events fulfilled the above criteria. Effect of above cuts are presented in fig. 28.

Contrary to negative particles, which are mainly pions, detected positive particles are a mixture of pions, kaons and protons. According to results from [8] positive kaons are expected to have shape similar to pions and their yield is about ten times less than pions. In detected events their admixture is even lower due to shorter kaon lifetime (fig. 3). Protons have higher momenta: their amount is about 2 times less than pions on 4 GeV/c, but they are more abundant than pions above 6 GeV/c. Ratio of protons to pions in accidental events was experimentally estimated in DIRAC up to 4 GeV/c by their TOF difference between forward detectors and the Vertical Hodoscope [9]. On the next stage of the DIRAC experiment [10] particle identification will be enhanced by dedicated aerogel and heavy-gas Cherenkov detectors. For the last reason this study will be restricted to the production shape of all positive hadrons in DIRAC kinematic range. This can be achieved, because acceptance functions for pions and protons are different by not more than 10% (if one use downstream detectors only) due to pion decays:

$$\frac{d^3N}{dpd\Theta d\varphi} = \frac{1}{G^{\pi^+}(p,\Theta,\varphi)}\frac{d^3N^{\mathrm{det}}_{\pi^+}}{dpd\Theta d\varphi} + \frac{1}{G^{K^+}(p,\Theta,\varphi)}\frac{d^3N^{\mathrm{det}}_{K^+}}{dpd\Theta d\varphi} + \frac{1}{G^{p}(p,\Theta,\varphi)}\frac{d^3N^{\mathrm{det}}_{p}}{dpd\Theta d\varphi}, \quad (9)$$

$$\frac{d^3N}{dpd\Theta d\varphi} \approx \frac{1}{G^{\pi^+}(p,\Theta,\varphi)}\frac{d^3N^{\mathrm{det}}}{dpd\Theta d\varphi}, \quad (10)$$

$$\frac{d^2N}{dpd\Theta} = \omega(p,\Theta)\int\limits_{\Omega^{\pi^+}} \frac{d^3N}{dpd\Theta d\varphi}d\varphi, \quad (11)$$

Fit parameters are presented in table 7. Simple formula (1), which was used as zero-approximation by the iterative method, does not reproduce experimental shape well (see fig. 29). But already the next iteration converges to fit parameters obtained by the method "G". Results of the more advanced tracking with Drift Chambers and more

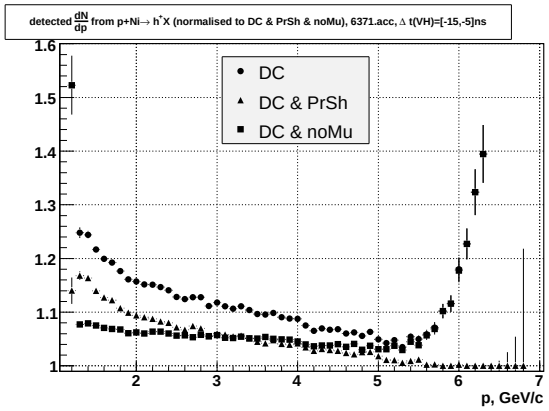

	criteria	N. events	
1.	DC(1 track)	250214	1
2.	1. & $\lvert\Delta t(\mathrm{PrSh})\rvert < 4$ ns	236483	0.95
3.	1. & no Muons	233855	0.93
4.	2. & no Muons	220259	0.88

Figure 28: Relative shape of $\dfrac{dN^{\mathrm{det}}}{dp}$ for different selection criteria.

Table 7: Fit parameters for h^+ production (TmTrxDC)

Particle		B	C_1	C_2 $[(\mathrm{GeV}/c)^{-1}]$	C_3 $[(\mathrm{GeV}/c)^{-2}]$	χ^2/NDF
$\{p \in [1.5,5]\mathrm{GeV/c}, \Theta \in [0.085,0.095]\}$ and $\{p \in [1.5,5]\mathrm{GeV/c}, \Theta \in [0.105,0.115]\}$						
h^+	G	4.69 ± 0.22	11.6 ± 0.6	-18.3 ± 2.6	12.4 ± 2.8	1740/1903
h^+	G^0	3.12 ± 0.15	7.0 ± 0.3	0.0	0.0	1819/1905
h^+	I1	5.66 ± 0.22	15.2 ± 0.6	-34.2 ± 2.6	26.4 ± 2.7	2055/1903
h^+	I2	4.96 ± 0.19	11.8 ± 0.6	-19.3 ± 2.5	11.4 ± 2.6	2027/1903

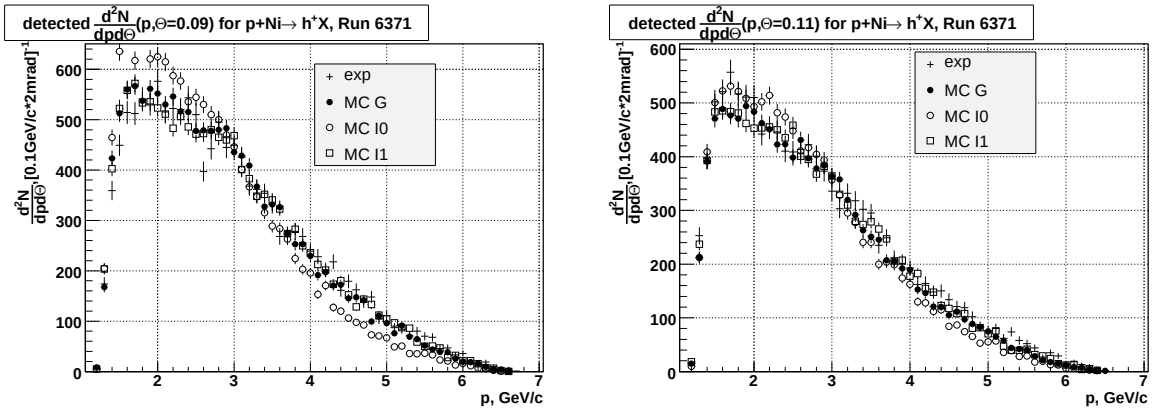

Figure 29: Detected $\dfrac{d^2N^{\mathrm{det}}}{dpd\Theta}\left(p + \mathrm{Ni} \to h^+X\right)$ for fixed values of Θ.

detailed map of the magnetic field ("noup") are presented in fig. 30 and table 8. As for negative pion production comparison of obtained production distributions with simplified and more advanced tracking (fig. 31-32) reveals background particles which appeared not in the target center: either as a decay product of long-lived particles (mainly kaons) or in interactions of the beam halo with the target, or particles burn/re-scattered in setup parts near the target.

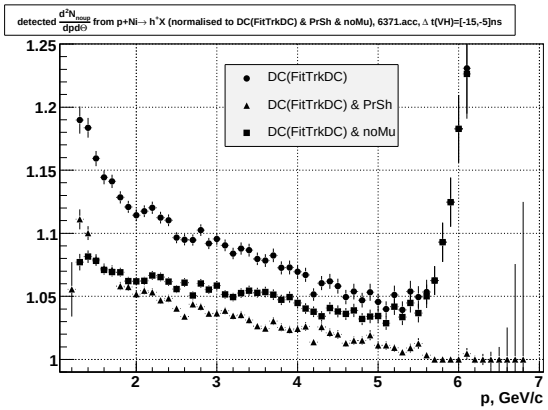

	criteria	N. events	
0.	DC(TmTrxDC)	250214	1.47
1.	DC(FitTrkDC)	170312	1
2.	1. & $\lvert\Delta t(\mathrm{PrSh})\rvert < 4$ ns	160832	0.94
3.	1. & no Muons	163583	0.96
4.	2. & no Muons	154182	0.91

Figure 30: Relative shape of $\dfrac{dN^{\mathrm{det}}_{\mathrm{noup}}}{dp}$ for different selection criteria.

Table 8: Fit parameters for h^+ production (FitTrkDC, DC only)

Particle		B	C_1	C_2 $[(\mathrm{GeV}/c)^{-1}]$	C_3 $[(\mathrm{GeV}/c)^{-2}]$	χ^2/NDF
$\{p \in [1.5,5]\mathrm{GeV}/c, \Theta \in [0.085,0.095]\}$ and $\{p \in [1.5,5]\mathrm{GeV}/c, \Theta \in [0.105,0.115]\}$						
h^+	G	3.15 ± 0.25	5.7 ± 0.7	6.4 ± 2.9	-9.0 ± 3.1	1721/1903
h^+	G^0	3.19 ± 0.17	6.8 ± 0.3	0.0	0.0	1730/1903

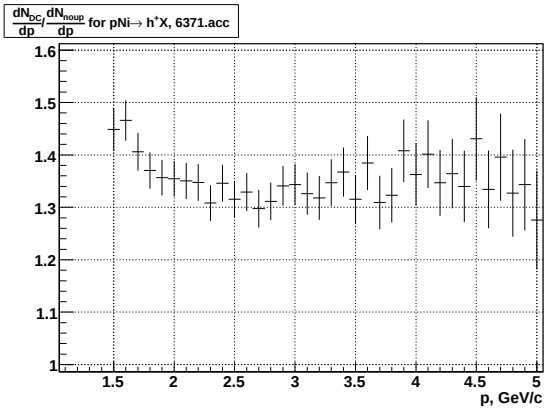

Figure 31: $\dfrac{dN_{\mathrm{DC}}}{dp} \Big/ \dfrac{dN_{\mathrm{noup}}}{dp}$.

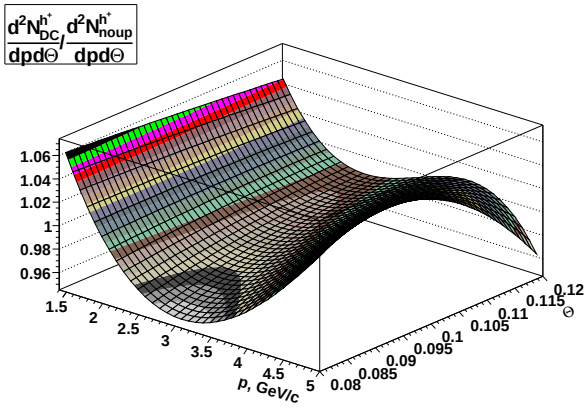

Figure 32: $\dfrac{d^2N_{\mathrm{DC}}}{dpd\Theta} \Big/ \dfrac{d^2N_{\mathrm{noup}}}{dpd\Theta}$.

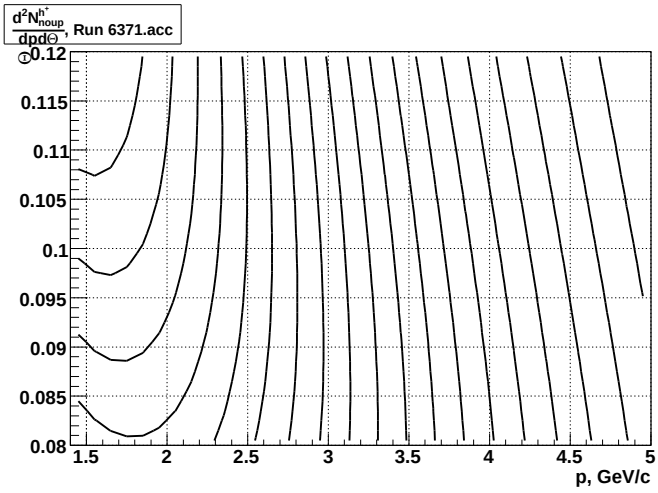

Figure 33: $\dfrac{d^2N_{\mathrm{noup}}}{dpd\Theta}$ for pNi $\to h^+X$.

2.3 Comparison to minimum-bias trigger

While selecting 2 separated in time tracks collected with "T1 $\pi^+\pi^-$ without coplanarity" trigger, we select positive or negative hadrons inclusively produced in proton collisions with nuclear target (pNi $\to h^{\pm}X$), but without inclusive pair production (pNi $\to h^+h^-X$), when both particles enter the Spectrometer acceptance. Rate of later events is rather small, nevertheless due to conservation laws particles from such pairs are expected to have softer momenta in comparison to particles inclusively produced in pNi $\to h^{\pm}X$ reaction. At the DIRAC spectrometer single particle inclusive production spectra can be collected if trigger issued only by single arm of the spectrometer. This was done with so-called "minimum bias" trigger $dE/dx \times V2$ when coincidence of a signal in the Vertical Hodoscope in the negative arm with a signal in the Ionisation Hodoscope was required.

Detected with the "minimum bias" trigger π^--spectra is slightly softer than the single π^--spectra collected with "T1 $\pi^+\pi^-$ without coplanarity" trigger (fig. 34). But one has take into account that run with the "minimum bias" trigger was collected in 2000 and run with the "T1 $\pi^+\pi^-$ without coplanarity" was collected in 2003. So this comparison might be biased due to different beam conditions (e.g. average proton beam intensity in run 6371 was about 20% higher than during run 2188).

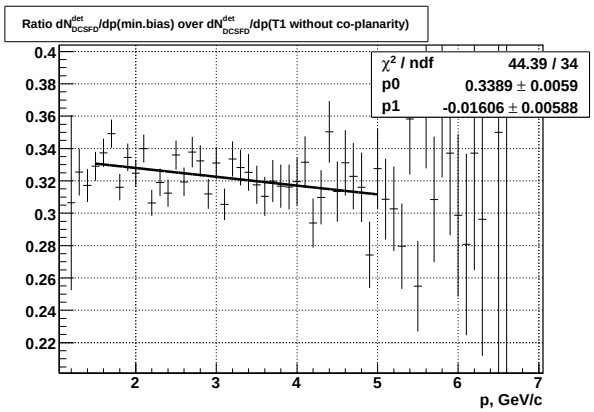

Figure 34: Ratio of $\frac{dN^{\rm det}_{\rm DC\&SFD}}{dp}$ for run 2188 ("minimum bias $dE/dx \times V2$") over the distribution for run 6371 ("T1 $\pi^+\pi^-$ without coplanarity") fitted by $p0(1 + p1 \cdot p)$.

2.4 Experimental spectra for 20/24 GeV/c

Part of DIRAC statistics was collected with proton beam momenta 20 GeV/c. Center-of-mass energy $\sqrt{s}$ in proton-nucleon collisions is lower by about 10%: from 6.84 GeV at 24 GeV/c to 6.27 GeV at 20 GeV/c. Detected distributions of accidental π^- collected with the "T1-coplanarity" trigger have similar shapes for 20 and 24GeV/c proton momenta runs (fig. 35). Where as the ratio of Badhwar parametrizations of the π^- inclusive production at different incident proton momenta is presented in fig. 36.

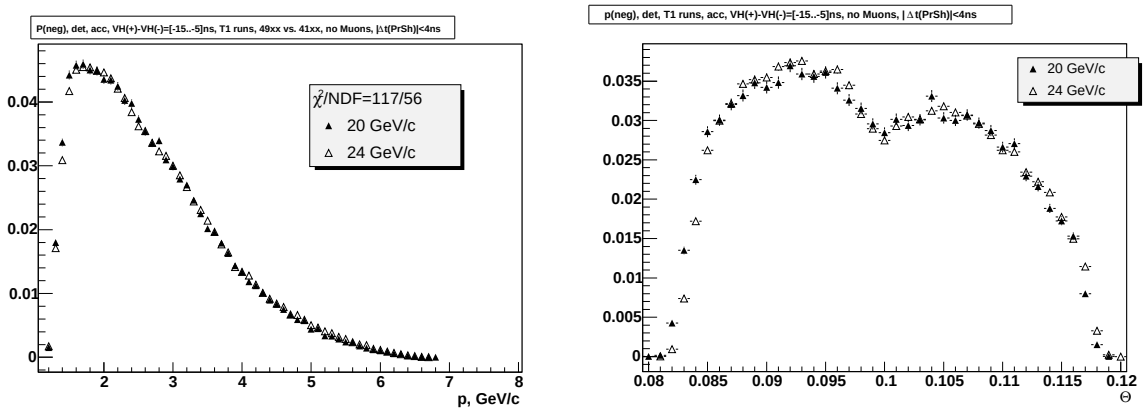

Figure 35: Detected π^- distributions on momenta p and polar angle Θ for different center-of-mass energies (normalised to have the same integral).

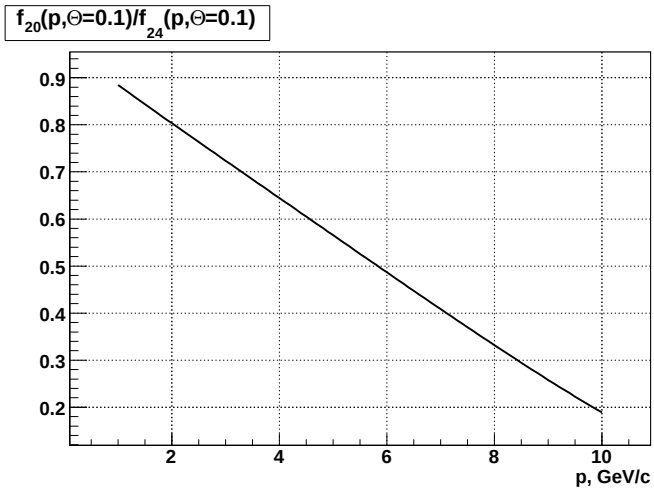

Figure 36: Ratio of Badhwar parametrizations of π^- inclusive production at incident proton momenta 20 GeV/c over 24 GeV/c as a function of π^--momenta.

3 Conclusions

Acceptance of the DIRAC setup has been defined by means of MC simulation as a 3-D function of incident single particle momenta ($\pi^{\pm}$, $K^{\pm}$ and protons). This 3-D description is complete, i.e. acceptance functions can be analytically transformed to different system of coordinates. Dependence of acceptance functions on different selection criteria has been studied.

Based on experimental data and above acceptance functions effective shapes of double differential production cross sections "on target" $\frac{d^2N}{dpd\Theta}$ for negatively or positively charged hadrons have been constructed, which reproduce (in Monte-Carlo simulation) detected by DIRAC experimental distributions. Double differential production cross section "on target" have been expressed in terms of compact analytical functions (so-called Badhwar parametrization). Momenta of incident protons is 24 GeV/c. Covered kinematic range of secondary particles is $p \in [1.5, 5.0]$ GeV/c and $\Theta \in [80, 120]$ mrad. These analytic effective shapes can be used to simulate accidental $\pi\pi$-pairs and to test validity of MC description of the DIRAC spectrometer.

Above double differential production cross section of negative pions from reaction pNi $\to \pi^- X$ does not fit experimental data obtained by Eichten et al. in the kinematic region common for both experiments. This difference can be partially explained by background of pions which appeared not in the target center but, for example, by the decay of secondaries or by interactions in spectrometer material. This source of uncertainties can be estimated (eliminated) by appropriate MC simulation. DIRAC acceptance covers about 6% of secondary pions from pNi collisions. This can be compared to about 12% of events of interest studied by Eichten et al. by scanning phase space. Instead DIRAC samples the available phase space continuously in a "single look". On the next stage of the DIRAC experiment particle identification will be enhanced by dedicated aerogel and heavy-gas Cherenkov detectors, which will make $\pi/K/p$-separation feasible. With the possibility to operate the DIRAC spectrometer magnet on several values of the magnetic field this makes the study of single-particle production by DIRAC competitive. Another possibility is to match our production shape "on target" to results of open-geometry hadroproduction experiments, which are now in the phase of data taking: e.g. MIPP (FNAL-E907) plans to measure particle production by proton beams between 5 and 120 GeV/c on various targets, including Cu.

* * *

This work would not have been possible without many members of the DIRAC team who shared their opinion for the problem and provided critical remarks, special thanks have to be addressed to Valery Yazkov for his invaluable help on different stages of this work.

A Spectra parametrization

To fit spectra we use parametrization of LIDCS[2] for $p+p \to \pi^{\pm} X$ suggested by Badhwar et al. [6]:

$$E\frac{d^3\sigma}{d^3p} = A_{\rm cs}\frac{(1-\tilde{x})^q}{(1+4m_p^2/s)^r}\exp\left[-Bp_\perp/(1+4m_p^2/s)\right], \tag{12}$$

$$\tilde{x} = \frac{E^*}{E^*_{\rm max}} \simeq \sqrt{x_\parallel^{*2} + \frac{4}{s}(p_\perp^2 + m_\pi^2)}, \quad x_\parallel^* = \frac{p_\parallel^*}{p^*_{\rm max}}, \tag{13}$$

$$q = \frac{C_1 + C_2 p_\perp + C_3 p_\perp^2}{\sqrt{1+4m_p^2/s}}. \tag{14}$$

Constants $A_{\rm cs}$, B, r, C_1, C_2, C_3 are free parameters. Fit over available experimental data gives values presented in Table 9.

Table 9: Parameters for representation of invariant cross sections [6]

Particle	$A_{\rm cs}$ [mb/(GeV$^2/c^3$)]	B	r	C_1	C_2 [(GeV/c)$^{-1}$]	C_3 [(GeV/c)$^{-2}$]
π^+	153	5.55	1	5.3667	−3.5	0.8334
π^-	127	5.3	3	7.0334	−4.5	1.667

For $p + N \to \pi^{\pm} X$:

$$\sigma_N^{\pm} = E\left.\frac{d^3\sigma}{d^3p}\right|_{pN\to\pi^{\pm}X} = A\frac{\lambda_{pp}}{\lambda_{pN}}\left[\sigma_\pm + \eta f_n(\sigma_\mp - \sigma_\pm)\right], \quad \text{where } \sigma_\pm = E\left.\frac{d^3\sigma}{d^3p}\right|_{pp\to\pi^{\pm}X}. \tag{15}$$

f_n is the fraction of neutrons in the target nucleus, λ_{pp} and λ_{pN} are the interaction mean free paths for pp and p-nucleus collisions. η is the charge mixing parameter.

Double differential production cross section $\dfrac{d^2\sigma}{dpd\Theta}$ can be expressed as

$$\frac{d^2\sigma}{dpd\Theta} = \frac{2\pi p^2 \sin\Theta}{E}\left.\left(E\frac{d^3\sigma}{d^3p}\right)\right|_{\rm Badhwar}. \tag{16}$$

[2]LIDCS — Lorentz invariant differential cross section

References

[1] A. Lanaro, *Parametrization of correlated and accidental particle spectra*, DIRAC internal note 2001-01.

[2] P. Zrelov, V. Yazkov, *The GEANT-DIRAC simulation program*, http://www.cern.ch/dirac.

[3] D. Drijard, M. Hansroul, V. Yazkov, *DIRAC offline reconstruction program Ariane*, http://www.cern.ch/dirac.

[4] B. Adeva et al. (DIRAC collaboration), *DIRAC: A high resolution spectrometer for pionium detection*, NIM A515 (2003) 467.

[5] A. Kulikov and M. Zhabitsky, *Dead time losses and their measurement in DIRAC*, NIM A527 (2004) 591.

[6] G.D. Badhwar, S.A. Stephens, and R.L. Golden, *Analytic representation of the proton-proton and proton-nucleus cross-sections and its application to the sea-level spectrum and charge ratio of muons*, Phys.Rev. **D15** (1977) 820.

[7] J.R. Sanford, C.L. Wang, BNL, AGS internal report, 1967, unpublished;
C.L. Wang, *Pion, Kaon, and Antiproton Production Between 10 and 70 BeV*, Phys. Rev. Lett. 25 (1970) 1068;
C.L. Wang, Phys. Rev. Lett. 25 (1970) 1536, Erratum.

[8] T.Eichten et al., *Particle production in proton interactions in nuclei at* 24 *GeV/c*, Nucl. Phys. B44 (1972) 333.

[9] S. Trusov, *Proton to pion ratio in accidental coincidences*, DIRAC internal note 2002-10.

[10] B. Adeva et al. (DIRAC collaboration), *Lifetime measurement of* $\pi^+\pi^-$ *and* $\pi^\pm K^\mp$ *atoms to test low energy QCD*, Addendum to the DIRAC proposal, CERN-SPSC-2004-009.